Research Article

GAZİ
JOURNAL OF ENGINEERING SCIENCES

# Design of a Frequency Selective Surface-Based Electromagnetic Absorber for X-Band Applications

Sena Esen Bayer Keskin[*a], Cem Güler[b], Erol Türkeş[c]

**Submitted:** 22.01.2026 **Revised:** 15.04.2026 **Accepted:** 15.04.2026 doi:10.30855/gmbd.070526N07

[a,*] Kırklareli University, Faculty of Engineering, Dept. of Electrical Electronics Engineering - Kırklareli, Türkiye, Orcid: 0000-0001-8309-3393
[b] Kırklareli University, Faculty of Engineering, Dept. of Electrical Electronics Engineering – Kırklareli, Türkiye, Orcid: 0000-0002-6631-7559
[c] Kırklareli University, Faculty of Engineering, Dept. of Mechanical Engineering – Kırklareli, Türkiye, Orcid: 0000-0002-9601-7119
*Corresponding author: senakeskin@klu.edu.tr*

**Keywords:** Frequency selective surfaces, absorber surfaces, X-band applications, narrowband

## ABSTRACT

This study presents a narrowband, low-profile frequency selective surface (FSS)-based electromagnetic absorber designed for X-band operation at 10 GHz. The proposed absorber aims to provide strong and selective absorption at a specific target frequency while maintaining a simple and practically feasible unit-cell configuration. In order to position the proposed design within the broader absorber literature, different electromagnetic absorber configurations, including flat-plate, quarter-wavelength (λ/4), multilayer, Jaumann, sawtooth/chevron, pyramidal, metamaterial-based, and FSS-based structures, are briefly evaluated in terms of their structural and frequency-dependent characteristics. This comparison shows that multilayer and broadband absorber configurations can improve bandwidth performance, but they generally introduce additional thickness, fabrication complexity, and cost. In contrast, FSS- and metamaterial-based absorbers offer greater geometric flexibility and can be tailored for narrowband, broadband, or multiband absorption responses. Building on this motivation, an original FSS-based absorber is proposed to achieve efficient absorption at 10 GHz, which is an important frequency region for radar, satellite, and high-frequency communication applications. The proposed unit cell consists of a central circular ring connected to four quarter-circular discs positioned at the corners. The structure is implemented on a 1.6 mm thick double-layer FR-4 substrate with a relative permittivity of 4.3, including a metallic top layer and a full conductive ground plane. The design is optimized and analyzed using CST Studio Suite with Floquet ports and periodic boundary conditions. The simulation results show that the proposed absorber achieves a peak absorptivity of 96.7% at 10 GHz and maintains absorptivity above 90% within the 9.95–10.06 GHz frequency range. These results indicate that the proposed design provides a simple, low-profile, and frequency-selective absorber solution for X-band applications.

## 1. Introduction

The rapid development of electronics, communication, and defense technologies has progressively increased the need for controlling electromagnetic waves. In many practical systems, including radar systems, satellite communications, high-frequency wireless communications, electromagnetic compatibility, sensor platforms, stealth technologies, and sensitive electronic systems, the suppression of reflections from incident electromagnetic waves has become increasingly important [1–3]. In this context, electromagnetic wave absorbers play a key role by attenuating incident energy within the structure rather than reflecting it back [4]. Their use is therefore important in applications such as electromagnetic interference suppression, radar cross-section reduction, anechoic chamber realization, and frequency-selective energy management

**To cite this article**: S. E. Bayer Keskin, C. Güler and E. Türkeş, "Design of a Frequency Selective Surface-Based Electromagnetic Absorber for X-Band Applications," Gazi Journal of Engineering Sciences, vol. 12, no. 1, pp. 97–111, 2026. doi: 10.30855/gmbd.070526N07

[5–8]. For this reason, absorber design should not be regarded as a limited problem based solely on appropriate material selection. Rather, it should be considered a multidimensional engineering subject that simultaneously addresses electromagnetic performance, frequency selectivity, structural robustness, manufacturability, and application requirements [9–11]. The performance of an electromagnetic absorber is fundamentally governed by two physical requirements: efficient impedance matching with free space [12–13], and sufficient dissipation of the incoming electromagnetic energy through conductive and dielectric losses [14]. When the input impedance of the absorber approaches the impedance of free space, reflection is minimized, and when transmission is suppressed by a conductive backing layer, the incident energy can be effectively absorbed within the lossy medium [15].

Among the earliest fundamental examples in the historical development of conventional microwave absorbers is the Salisbury screen [16], which employs a resistive sheet positioned approximately one quarter wavelength away from a conductive ground plane. Although it is effective around the resonance frequency, it exhibits a narrowband operating characteristic and suffers from significant thickness-related limitations, especially in applications requiring a low-profile configuration [17]. To overcome this limitation, multilayer configurations, such as the Jaumann absorber, were developed to enhance bandwidth. [18]. However, the increase in bandwidth generally comes at the expense of greater structural thickness and design complexity. These trade-offs have motivated growing interest in frequency selective surface (FSS)- and metamaterial-based absorbers, which offer thinner profiles, reduced weight, and greater flexibility in controlling electromagnetic behavior through periodic metallic patterns [19–26]. In FSS- and metasurface-based absorbers, the geometry of the unit cell plays a decisive role in determining resonant behavior and absorption performance. Parameters such as shape, size, symmetry, and the coupling between adjacent elements directly influence the equivalent inductive and capacitive behavior of the structure, and hence its frequency response [27]. This geometric controllability has enabled the development of absorber designs with narrowband, broadband, multiband, and ultra-wideband characteristics. At the same time, literature shows that high-performance absorption is frequently achieved by multilayer configurations, resistively loaded elements, air gaps, or complex multi-resonant elements [28–38]. While such strategies may improve bandwidth or angular stability, they also tend to increase fabrication difficulty, structural complexity, and integration cost.

It should also be emphasized that broadband absorption is not the objective in every absorber application. In many practical systems, the primary requirement is not to suppress a very wide frequency range, but rather to achieve strong and selective absorption behavior around a specific target frequency. In particular, narrowband absorbers are especially relevant in applications involving frequency-selective reflection control, narrow-spectrum suppression, reduction of the electromagnetic signature in specific radar or communication channels, and systems optimized around a single center frequency [39]. Therefore, the performance of an absorber should not be evaluated solely in terms of bandwidth, but also in terms of peak absorption level at the target frequency, structural simplicity, low profile, material availability, ease of fabrication, and angular and polarization stability. Within this framework, the X-band is widely used in radar, satellite communications, high-frequency sensing, imaging, and various defense electronics applications [40]. Narrowband absorbers operating around 10 GHz offer an effective solution for systems that require strong absorption and controlled reflection reduction at a target frequency. When absorber designs proposed for the X-band or around 10 GHz are examined, it becomes clear that most studies are concentrated around several main directions. The first of these is the use of multilayer or air-spaced configurations to increase bandwidth. In this context, Sohrab and Atlasbaf presented a multilayer absorber design consisting of two RO4003 layers separated by a 1.4 mm air gap, with a total thickness of 3 mm. The proposed structure provides a 40% bandwidth for 20 dB across the X-band, thus exhibiting broadband performance. However, this bandwidth enhancement is accompanied by a more complex physical structure and a more sensitive fabrication process due to the use of a multilayer configuration, an air gap, and resistively loaded elements [41]. Syihabuddin et al. presented a multilayer metasurface absorber design for the X-band. The structure consists of an SRR in the lower layer, a thin narrow strip in the upper layer, and a 0.8 mm FR-4 substrate within a $3.8 \times 3.8$ mm$^2$ unit cell. By varying the interlayer spacing or dielectric separation from 0.1 to 1.0 mm, the resonance was shown to lie approximately within the 9.26–9.68 GHz range, while the maximum bandwidth was reported to be about 0.12 GHz. The study demonstrates bandwidth enhancement through a multilayer structure [42]. Yüzer and Erdem proposed a textile-based three-layer metamaterial absorber for the X-band. The structure consists of a Z-shaped conductive resonator on the top, a silicone dielectric layer in the middle, and a conductive surface at the bottom. Copper was used as the conductive layer, with a conductor thickness of 50 μm, while the relative permittivity of the silicone layer was 11.9. By varying the silicone

layer thickness between 1.2 and 2.0 mm, the best result was obtained at a thickness of 1.6 mm, yielding a maximum absorption of 90.72% at 10.40 GHz. The study shows that increasing dielectric thickness shifts the resonance frequency toward lower frequencies, while the maximum absorption remains nearly unchanged [43]. A second direction involves the introduction of resistive loading or artificial loss mechanisms to increase the absorption level. For example, Pelluri and Appasani designed an FR-4-based X-band absorber with an irregular patch arrangement optimized by a genetic algorithm and reported 97% absorption over the 10.42–11.98 GHz range, with a peak absorption of 99.95% at 10.52 GHz. However, compared with simple and classical resonator geometries, such optimization-based approaches require greater computational cost and a more complex design process [44]. In the same line, Abdalla and Hu proposed fan-shaped SRR and modified high-impedance-surface-based absorber structures as alternatives to the conventional rectangular SRR configuration. Their study showed that the fan-shaped SRR design significantly increases bandwidth around 9.5 GHz compared with the conventional SRR, while also creating a second absorption band around 11.7 GHz. Likewise, another modified grooved-patch high-impedance structure achieved a 10 dB bandwidth of approximately 9.5–10.5 GHz around the 10 GHz center frequency and was reported to operate under both co-polarized and cross-polarized waves [45]. However, such performance improvements generally come at the cost of more complex resonator geometries, asymmetric slot arrangements, conductive pin connections, and resistor integration, all of which complicate the design and fabrication process. For this reason, there remains a need in the literature for balanced absorber designs that exhibit simple geometry, low profile, easy implementation using conventional printed circuit technologies, and high absorption at the target frequency.

In this study, a narrowband, low-profile, FSS-based electromagnetic absorber operating at 10 GHz is proposed for X-band applications. The unit cell consists of a central circular ring connected to four quarter-circular elements positioned at the corners, forming a compact and symmetric geometry. The structure is implemented on a 1.6 mm thick double-layer FR-4 substrate backed by a full conductive ground plane, and its electromagnetic behavior is analyzed in CST Studio Suite under Floquet ports and periodic boundary conditions. Simulation results show that the proposed absorber exhibits a peak absorption of approximately 96.7% at 10 GHz and maintains absorption above 90% over the 9.95–10.06 GHz range. A bandwidth of approximately 112 MHz and a fractional bandwidth of 1.12% clearly reveal the pronounced narrowband character of the structure. To explain the absorption mechanism, not only the frequency response but also the equivalent circuit model, parametric analyses, surface current distributions, and electric-field concentrations were examined. The findings indicate that the high absorption arises from the combined effect of resonance, impedance matching, and loss mechanisms. In addition, the evaluation of the response under different incidence angles supports the application potential of the design. From this perspective, the study offers a strong, selective, structurally simple, and practically feasible absorber solution around 10 GHz as an alternative to broadband but more complex configurations.

## 2. Design and Simulation

In this paper, an original absorber design is introduced to effectively absorb electromagnetic waves in the X band, specifically at 10 GHz. This frequency is particularly significant due to its extensive applications in radar, satellite and high-frequency communication systems, where efficient absorption is essential to mitigate interference and enhance performance. The unit cell of the absorber features a circular ring centrally positioned within the cell with four quarter-circular discs situated at the corners, each connected to the central ring. The FSS unit cell configuration is placed on a 1.6 mm thick double-layer FR-4 dielectric substrate with a dielectric constant of 4.3, featuring a metallic structure on the top and a full ground plane at the bottom. The absorber's unit cell dimension parameters have been optimized and depicted in Figure 1. Here, $d_w = 13\,mm, R_r = 10\,mm, r = 8.4\,mm, r_r = 4.57\,mm, h = 1.6\,mm, and\ t = 0.035\,mm.$ Comprehensive analysis of the unit cell's characteristics and performance has been conducted using CST Studio Suite, employing Floquet ports and periodic boundary conditions to simulate the electromagnetic response accurately.

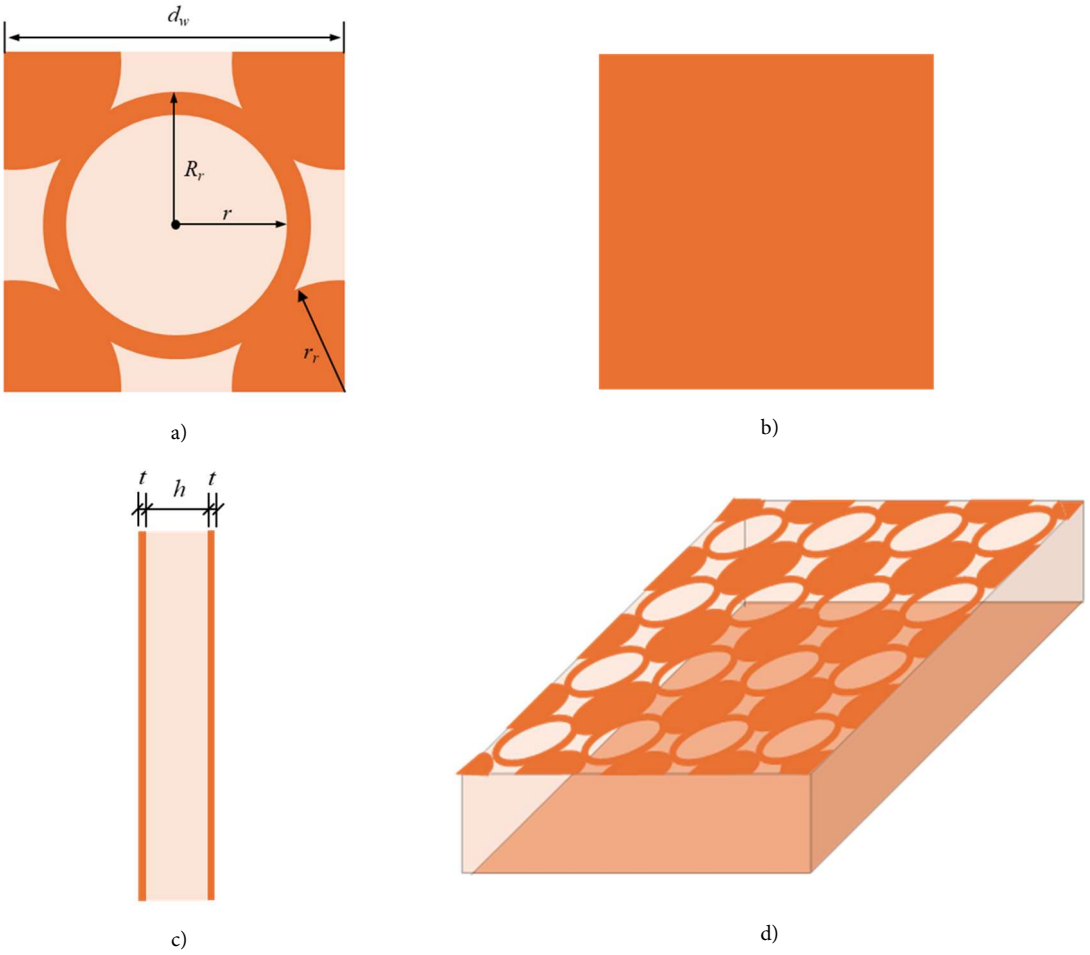


Figure 1. Unit Cell Dimensions of the Proposed Absorber a) top view, b) bottom view, c) side view, and d) perspective view.

Mathematically, the absorption performance of the absorber is expressed by Equation (1):

$$A = 1 - |S_{11}|^2 - |S_{21}|^2 \quad (1)$$

where A stands for absorptivity, and $S_{11}$ and $S_{21}$ represent the reflection and transmission coefficients, respectively. Due to the presence of the PEC (Perfect Electric Conductor) back-plane, the transmission coefficient $S_{21}$ is zero. Therefore, Equation (1) can be rewritten as follows:

$$A = 1 - |S_{11}|^2 \quad (2)$$

The simulation, optimization, and parametric study of the absorber are performed using CST Microwave Studio software. The absorptivity graph for the simulated absorber is depicted in Figure 2. According to the simulation data, it exhibits a bandwidth of 112 MHz between the frequencies 9.95 GHz and 10.06 GHz, with absorption levels exceeding 90% throughout this frequency range with a nearly perfect absorption of over 96.7% at 10 GHz. Also Figure 2 shows that the proposed absorber reaches a peak absorptivity of 96.7% at 10 GHz and maintains absorptivity above 90% within the 9.95–10.06 GHz frequency range. This corresponds to a bandwidth of 112 MHz around the center frequency. When evaluated in terms of fractional bandwidth, this value corresponds to approximately 1.12%, indicating that the proposed structure exhibits a narrowband absorption characteristic. This behavior is consistent with the selected unit-cell topology, where the absorption response is mainly governed by a dominant single-resonance mechanism rather than multiple overlapping resonances. From an application perspective, such a narrowband response is suitable for systems requiring frequency-selective absorption within a well-defined portion of the X-band, rather than broadband suppression over a wide

frequency interval.

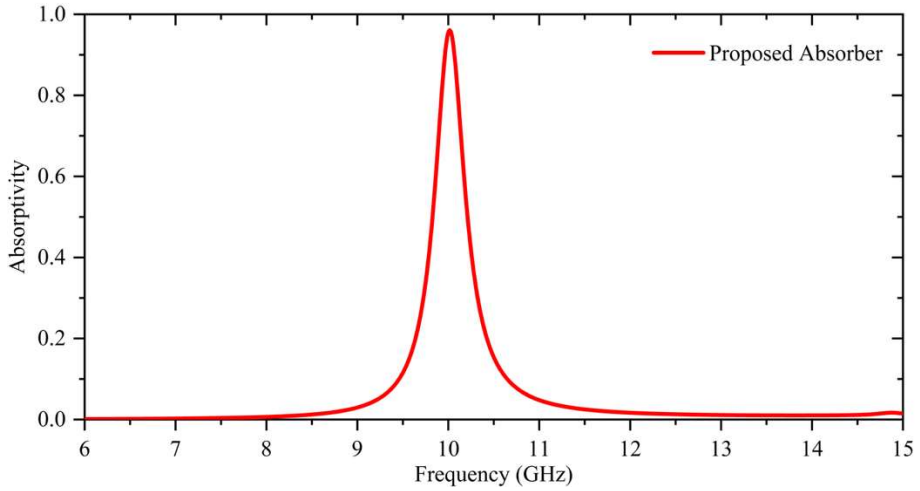


Figure 2. Simulated absorption.

In Figure 3, the absorption and reflection graphs of the absorber design are presented, demonstrating its effectiveness in absorbing and reflecting electromagnetic waves within the frequency range of 9.95-10.06 GHz. This frequency range falls within the X band, which spans from 8 to 12 GHz. Notably, the absorption coefficient peaks at 96.7% absorption at the central frequency of 10 GHz. Such high performance makes the absorber well-suited for applications requiring precise absorption and reflection control in the X band, including radar systems, communication networks, and stealth technology.

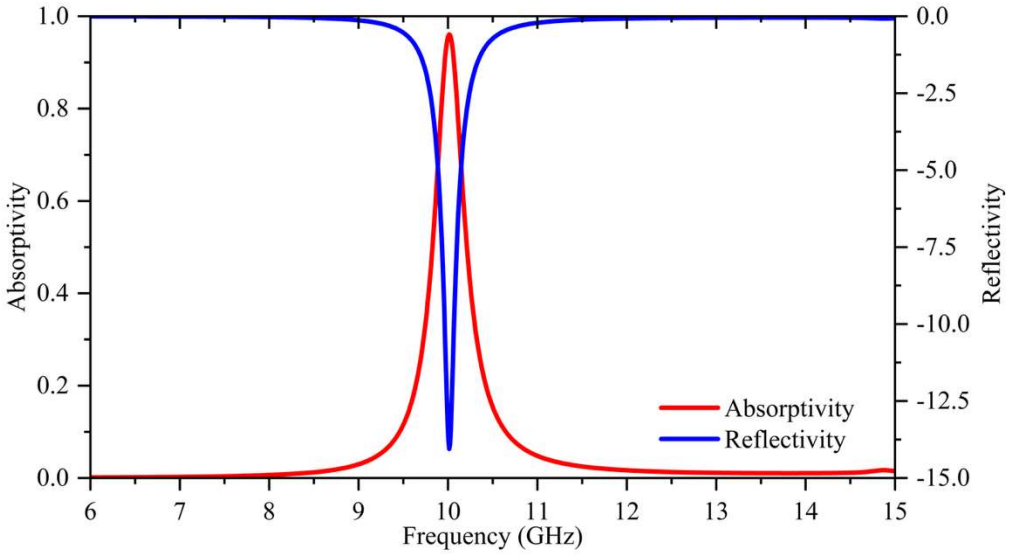


Figure 3. The absorptivity and reflectivity graphs of the proposed design.

To provide a clearer physical interpretation of the absorption mechanism of the proposed absorber, a lumped-element equivalent circuit model (ECM) was developed, as illustrated in Figure 4. In this model, the metallic sections responsible for current flow are represented by inductive elements, whereas the capacitive coupling between adjacent metallic parts is modeled by a lumped capacitor. In addition, the ohmic and dielectric losses are considered by a lumped resistance. Accordingly, the dominant resonant path of the absorber is modeled by a series $R_1$-$L_1$-$C_1$ branch, while the additional current path associated with the remaining metallic section is represented by an inductive branch $L_2$.

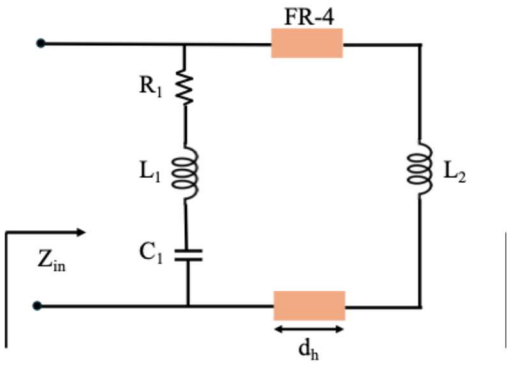


Figure 4. Lumped-element equivalent circuit model of the proposed X-band absorber.

Based on the extracted circuit parameters, the element values were determined as $R_1 = 5\ \Omega$, $L_1 = 2.29$ nH, $C_1 = 0.1$ pF, and $L_2 = 0.26$ nH. The impedance of the main resonant branch can therefore be written as [46,47]

$$Z_1 = R_1 + j\omega L_1 + \frac{1}{j\omega C_1}, \tag{3}$$

where $R_1$ represents the effective loss mechanism, $L_1$ corresponds to the inductive current path formed along the metallic resonator, and $C_1$ accounts for the electric-field coupling concentrated in the narrow gap regions. The impedance of the secondary branch is expressed as

$$Z_2 = j\omega L_2, \tag{4}$$

where $L_2$ models the additional inductive contribution of the outer metallic path. Since these two branches are connected in parallel, the total input impedance of the equivalent circuit is given by

$$Z_{in} = \left(\frac{1}{Z_1} + \frac{1}{Z_2}\right)^{-1} \tag{5}$$

The reflection coefficient can then be expressed in terms of the input impedance as

$$\Gamma = \frac{Z_{in} - Z_0}{Z_{in} + Z_0} \tag{6}$$

where $Z_0$ is the free-space impedance, equal to 377 Ω. Because the proposed absorber is backed by a metallic ground plane, the transmission coefficient is zero ($S_{21} = 0$), and thus the absorptivity is governed only by the reflection coefficient:

$$A(\omega) = 1 - |\Gamma|^2 \tag{7}$$

The main resonance frequency of the ECM is primarily determined by the $L_1C_1$ combination and can be approximated as [48],

$$f_r = \frac{1}{2\pi\sqrt{L_1 C_1}} \tag{8}$$

By substituting $L_1 = 2.29$ nH and $C_1 = 0.1$ pF into Eq. (8), the resonance frequency is calculated to be approximately 10.5 GHz, which is reasonably close to the full-wave simulated absorption peak observed around 10 GHz. This agreement confirms that the proposed ECM successfully captures the dominant resonant behavior of the absorber.

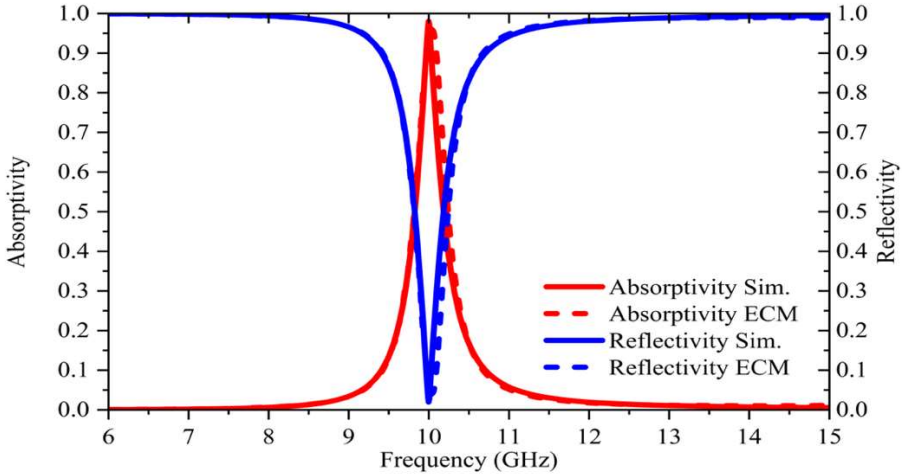


Figure 5. Absorptivity and reflectivity responses simulation and obtained from the equivalent circuit model.

From a physical point of view, the inductive components $L_1$ and $L_2$ represent the current loops formed on the metallic pattern, whereas the capacitor $C_1$ describes the localized electric-field storage between closely spaced conducting regions. The resistor $R_1$ plays an important role in modeling the dissipation of the incident electromagnetic energy through conductor and dielectric losses. At resonance, the inductive and capacitive reactances tend to compensate each other, causing the input impedance of the structure to approach the free-space impedance. Under this condition, the reflection coefficient is minimized, and the incident energy is largely dissipated inside the absorber rather than being reflected. Therefore, the high absorptivity obtained near 10 GHz can be attributed to the combined effect of resonance, impedance matching, and loss-assisted energy dissipation. Figure 6 shows the developing stages of the absorber design. Absorber I has only a circular ring in the center, whereas Absorber II incorporates quarter-circular disks positioned at opposite corners. The third stage of the design introduces the absorber structure proposed in this study, demonstrating its functionality within the desired frequency range.

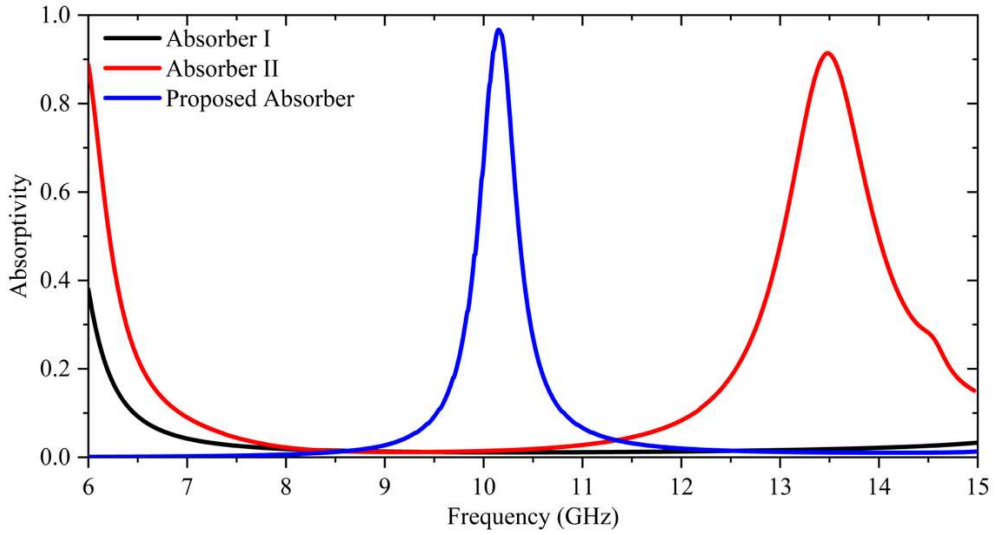


Figure 6. Evolution of FSS absorber design stages.

To achieve absorption in the X-band at the 10 GHz resonance frequency, a parametric analysis of the proposed geometry is conducted. Initially, the absorptivity for different values of the variable (h), representing the height of the dielectric substrate, is analyzed. The results of this analysis, along with corresponding data, are presented in Figure 7.

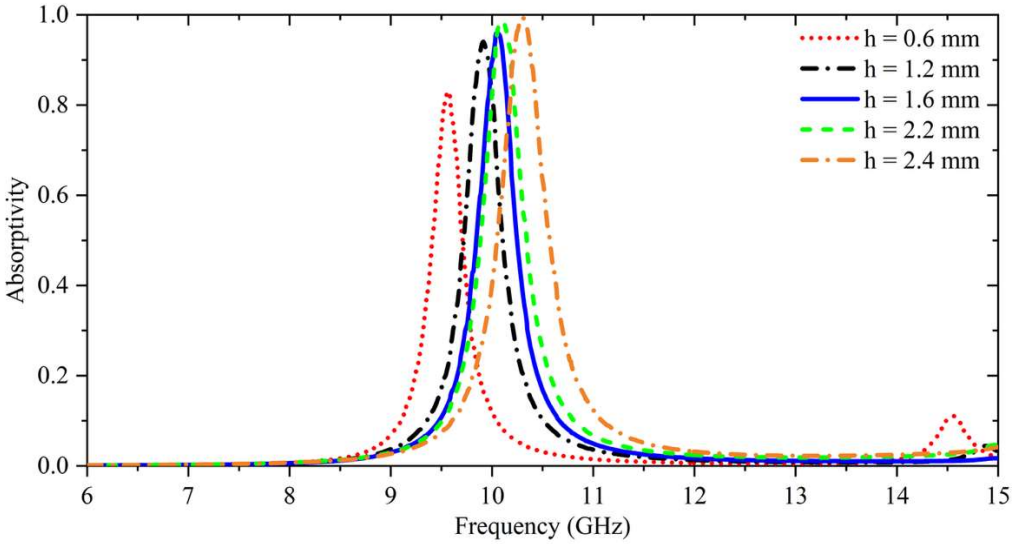


Figure 7. Absorptivity analysis for various heights (h) of the dielectric substrate.

Figure 8 illustrates the impact of dielectric properties on absorber performance using four different materials: FR-4, RT/Duroid 5880, Arlon AD600, and RT/Duroid 6010 LM, with a constant layer height (h=1.6 mm). The results highlight the significant influence of dielectric coefficient on absorber performance. In the X-band frequency range (8 GHz - 12 GHz), FR-4 material demonstrates the highest absorption rate (98%). Conversely, RT/Duroid 5880, with a dielectric constant of 2.2, achieves 11% absorption in the 13 GHz region. Arlon AD600, with a dielectric constant of 6.15, exhibits absorption below 60% in the 6 GHz and 14 GHz regions. RT/Duroid 6010 LM, featuring a dielectric coefficient of 11.2, offers absorption below 60%. Additionally, FR-4 offers advantages such as low cost, widespread availability, and ease of fabrication, making it a favorable choice for various applications.

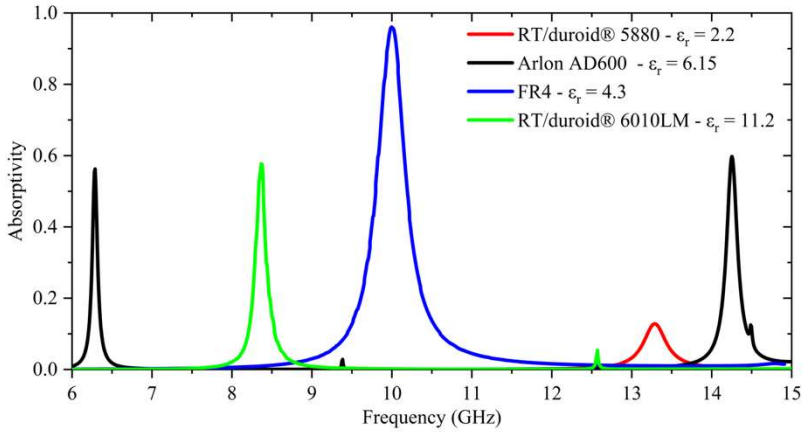


Figure 8. Impact of dielectric properties ($\varepsilon_r$) on absorber performance.

To examine the absorption rate of the copper material utilized in the absorber design, the graph illustrating the variation of copper thickness, as depicted in Figure 9, is analyzed.

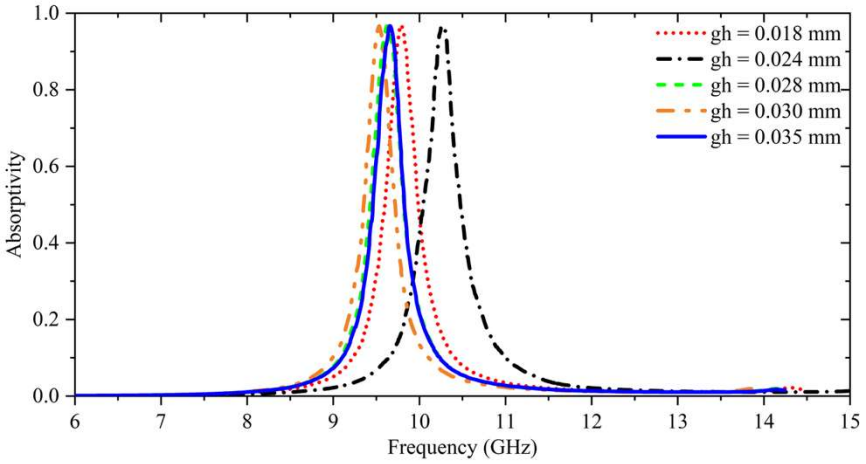


Figure 9. Absorptivity analysis for various copper thickness (gh)

In order to optimize the geometric dimensions of the unit cell, the impact of the radius of the centered circle on absorption performance is examined. This analysis considers various values of the radius, as depicted in Figure 10. The analysis indicated that at gh = 4.2 mm, the absorber exhibited the highest absorption rate within the desired frequency range.

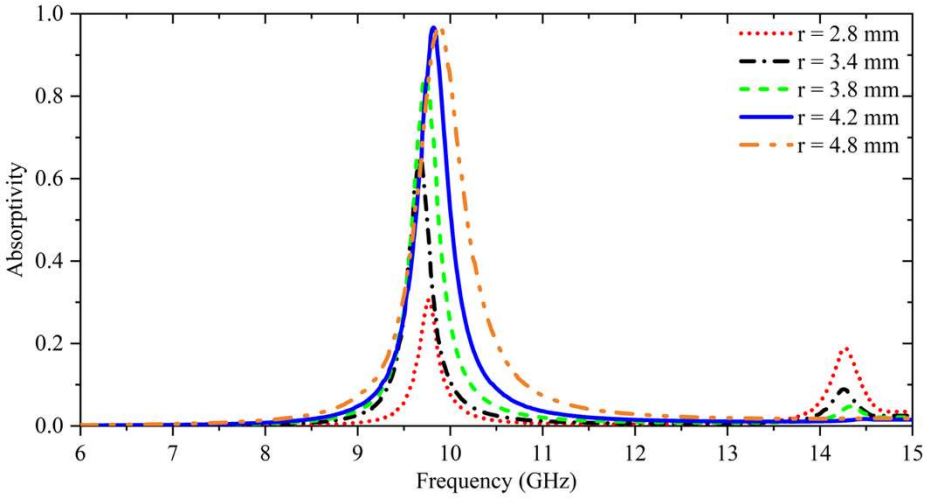


Figure 10. Impact of circular ring radius (r) on absorption performance

To enhance the absorption capacity of the unit cell, we explore the impact of varying the size of the semicircles placed at the corners. This investigation aims to understand how changes in semicircle size influence absorption ability. The choice of $r_r$ = 4.1 mm stems from the superior results depicted in Figure 11, where the absorber demonstrated its highest absorption performance.

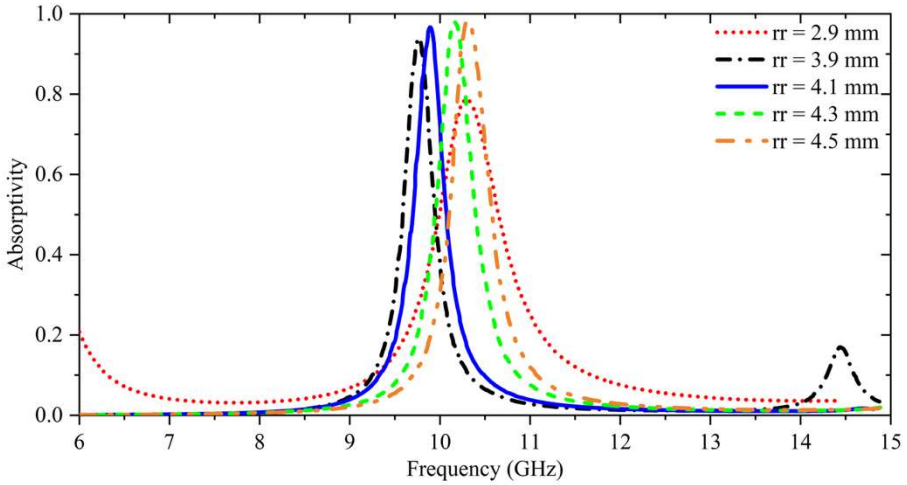


Figure 11. Impact of quarter-circular disc's radius (rr) on absorption performance

The surface current distribution and electric field distribution play crucial roles in evaluating absorber performance. At a frequency of 10 GHz, the current density within the designed absorber structure is observed to intensify notably at the intersection points between the central circle and the quarter circles at the edges. Figure 12 depicts both the surface current distribution and the electric field distribution of the designed unit cell, offering insights into the electromagnetic behavior of the absorber at this frequency.

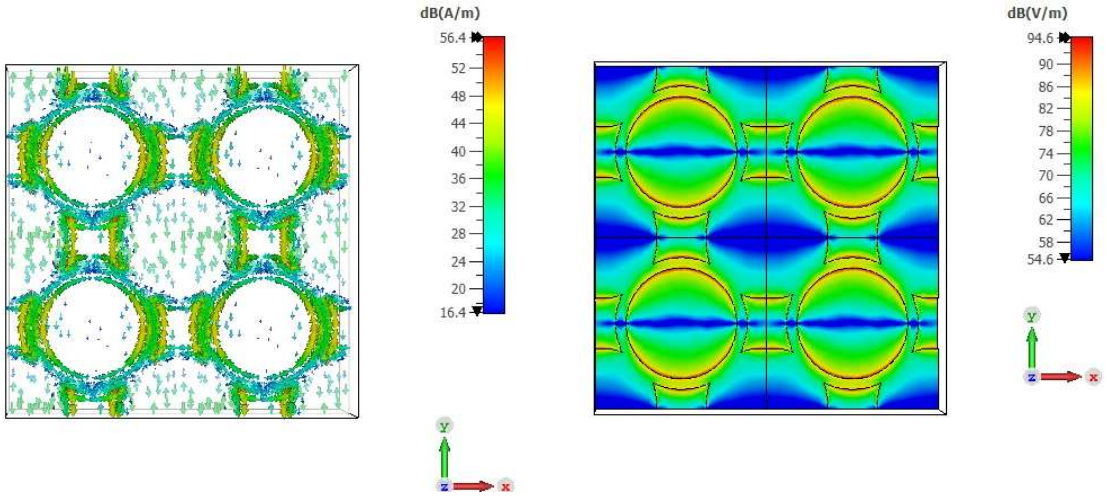


(a) (b)

Figure 12. (a) Surface current distribution at the resonance frequency of the unit cell, (b) Induced electric field at the resonance frequency of the unit cell structure.

Critical features of electromagnetic absorbers encompass polarization independence and a broad operating angle. Ideal absorbers should seamlessly accommodate various polarizations and span a wide range of incident angles. In this study, the absorber's performance is analyzed for both TE (Transverse Electric) and TM (Transverse Magnetic) modes at various angles of incidence (θ), as illustrated in Figure 13 and 14, respectively. The results demonstrate stable performance for both TE and TM polarizations, with the absorber maintaining effectiveness up to 60° along the absorption band. The distributions presented in Figure 12 provide a clearer physical interpretation of the absorption mechanism at the resonance frequency of 10 GHz. As shown in the surface current distribution, the induced current is mainly concentrated around the junction regions between the central circular ring and the quarter-circular corner elements. This behavior indicates that these regions form the dominant resonant current path of the unit cell. At the same frequency, the electric field is strongly localized in the narrow coupling regions, revealing increased capacitive field confinement between adjacent metallic parts. The combined presence of inductive current circulation and localized capacitive coupling

establishes the resonance condition responsible for the observed absorption peak. Since the structure is backed by a metallic ground plane, transmission is suppressed, and the incident electromagnetic energy is primarily dissipated through dielectric and conductor losses after the input impedance approaches that of free space. Therefore, the absorption mechanism of the proposed design can be attributed to the resonant interaction between the circular ring and the corner elements, together with improved impedance matching at the target frequency.

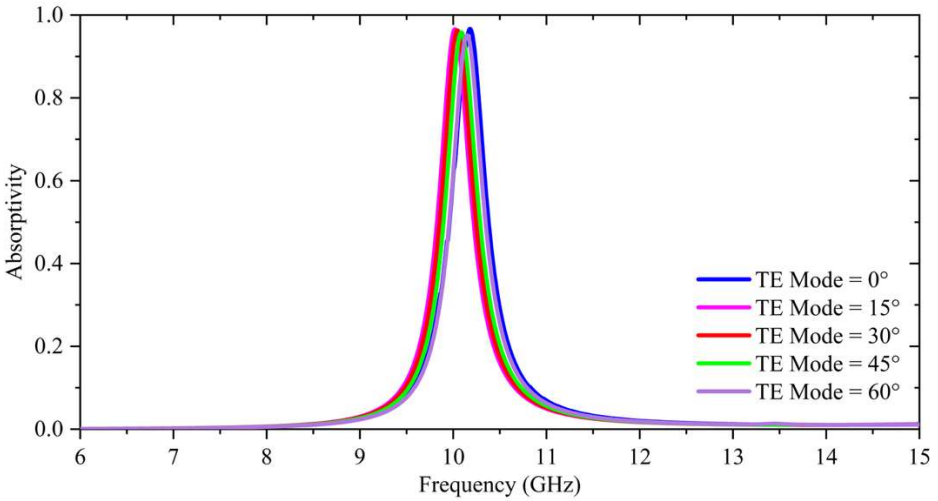


Figure 13. Absorption at various angles of incidence (θ) for TE Mode.

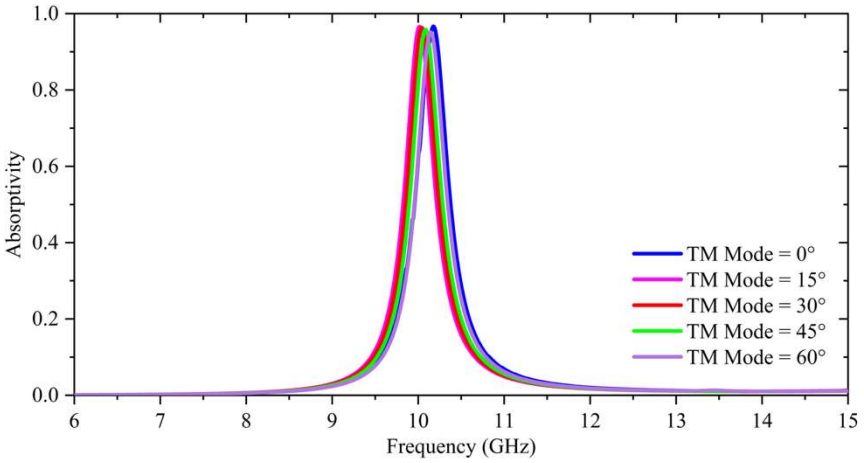


Figure 14. Absorption at various angles of incidence (θ) for TM Mode.

To more clearly demonstrate the originality and technical positioning of the proposed absorber, a comparative evaluation with representative FSS/metamaterial absorber studies operating in the X-band or around 10 GHz is presented in Table 1. As seen from the literature, previous studies have mainly focused on broadband absorption, multilayer configurations, resistor-loaded structures, or multi-band responses. For example, [44] reported a GA-optimized FR-4 absorber with very high peak absorptivity, but the structure was polarization-sensitive and stable only up to 30° incidence. Similarly, [41] introduced a wideband circuit analog absorber with air gap and resistor loading, although this was achieved by a thicker and more complex multilayer configuration. In contrast, [21] proposed an ultrathin absorber with good polarization and angular stability, yet its peak absorptivity remained lower than that of the present work. Other studies such as [45] and [42] mainly emphasized bandwidth enhancement through modified high-impedance or multilayer metasurface configurations, but these approaches required more complex structural arrangements and did not always report a complete set of polarization and angular stability metrics. Likewise, [22] and [43] relied on resistor-loaded concepts for improving absorption behavior, while [24] focused on a textile-based absorber whose peak absorptivity remained relatively limited. In addition, [25] presented a thin dual-band absorber with favorable angular and polarization

performance, but its operating principle was based on dual-band behavior rather than a compact and selective single-band response. Therefore, the comparison in Table 1 is intended to clarify the relative strengths, limitations, and trade-offs of earlier X-band absorber designs and to position the proposed absorber more explicitly within this context.

TABLE 1. Literature comparison of representative X-band FSS/metamaterial absorbers and the proposed design

| Parameter | [21] | [22] | [24] | [25] | [41] | [42] | [43] | [44] | [45] | [This work] |
|---|---|---|---|---|---|---|---|---|---|---|
| ***Structure*** | *Cross-shaped metasurface absorber* | *Resistor-loaded single-layer FSAS* | *Resistor-loaded wideband MMA* | *Dual-band FSS absorber* | *Two-layer CAA with air gap* | *Multilayer SRR absorber* | *Textile-based Z-shaped absorber* | *GA-optimized FR-4 absorber* | *Slotted-patch HIGP absorber* | *FSS-based narrowband absorber* |
| ***Resonance Frequency (GHz)*** | *10.48* | *8.28* | *Not reported* | *9 / 12.2* | *10* | *9.5* | *10.40* | *10.52* | *10* | *10* |
| ***Peak Absorptivity (%)*** | *97* | *Not reported* | *90* | *90* | *Not reported* | *Not reported* | *90.72* | *99.95* | *Not reported* | *96.7* |
| ***Absorption Bandwidth*** | *10.24-10.72 GHz* | *10.94%* | *Not reported* | *Not reported* | *2 GHz* | *0.12 GHz* | *Not reported* | *8-9 / 9.35-12 GHz* | *9.5-10.5 GHz* | *9.95-10.06 GHz* |
| ***Thickness (mm)*** | *0.8* | *1.6* | *3.07* | *0.8* | *3* | *2.4* | *1.6* | *1.58* | *1.6* | *1.6* |
| ***Substrate*** | *FR-4* | *FR-4* | *FR-4* | *FR-4* | *Rogers RO4003 + air gap* | *FR-4* | *Textile + silicone* | *FR-4* | *FR-4* | *FR-4* |
| ***Polarization Stability*** | *Independent* | *Insensitive* | *Insensitive* | *Insensitive* | *Single-polarized* | *Not reported* | *Not reported* | *TE-polarized* | *Co-/cross-polarized* | *TE/TM stable* |
| ***Angular Stability*** | *60°* | *30°* | *Limited, TE 40°* | *60°* | *45°* | *Not reported* | *Not reported* | *30°* | *Not reported* | *60°* |

As summarized in Table 1, previously reported X-band absorbers generally achieve their performance by prioritizing one of several design directions, including broadband absorption [24,41,44] multilayer or structurally modified configurations [42,45], resistor-loaded implementations [22,24,41], textile-based flexible concepts [43], or dual-band operation [25]. Although some of these studies provide advantages such as high peak absorption, wider operating bandwidth, or ultrathin profiles, they often involve trade-offs in the form of increased structural complexity, air gaps, lumped resistors, multi-band behavior, incomplete angular/polarization characterization, or limited absorption stability. In this respect, the proposed absorber offers a balanced and practically attractive alternative. Unlike many earlier studies, it employs a simple FSS-based narrowband configuration on an FR-4 substrate with a low profile of 1.6 mm, while still providing 96.7% peak absorptivity at 10 GHz and stable performance for both TE and TM polarizations up to 60° incidence. Accordingly, the main contribution of this work is not to maximize bandwidth, but to realize a structurally simple, low-profile, and experimentally practical X-band absorber that combines strong absorption with robust angular and polarization stability.

## 3. Conclusion

This study presents the electromagnetic performance analysis of the proposed FSS-based absorber for X-band applications at 10 GHz. The analysis indicates that each absorber configuration provides certain advantages depending on the intended operating frequency range, structural complexity, and application requirements. Based on the findings obtained from this comparative evaluation, a novel FSS-based absorber was designed and optimized for X-band operation at 10 GHz. The proposed structure consists of a circular ring and four quarter-circular discs implemented on a 1.6 mm thick double-layered FR-4 substrate backed by a metallic ground plane. Full-wave simulations carried out in CST Studio Suite show that the proposed absorber achieves a peak absorptivity of 96.7% at 10 GHz and maintains absorptivity above 90% within the 9.95–10.06 GHz frequency range, corresponding to a bandwidth of 112 MHz. These results demonstrate that the proposed design provides effective absorption at the target frequency while preserving a geometrically simple and low-profile configuration. In addition to the numerical absorption response, the parametric analyses reveal that the resonance behavior is strongly influenced by the geometric dimensions of the circular ring and the corner elements, since these parameters directly determine the effective current path length and the electromagnetic coupling within the unit cell. In

particular, the analysis shows that the optimum absorption performance is obtained when the radius of the circular ring is selected as 4.2 mm and the radius of the quarter-circular corner elements is chosen as 4.1 mm. Variations in these geometrical parameters result in shifts in the resonance frequency as well as changes in the absorption level. The effect of substrate material was also investigated in detail. For a fixed substrate thickness of 1.6 mm, FR-4 provided the highest absorption performance, reaching approximately 98% within the X-band region. In contrast, RT/Duroid 5880, with a dielectric constant of 2.2, exhibited only 11% absorption around 13 GHz. Similarly, Arlon AD600 and RT/Duroid 6010LM remained below 60% absorption in the examined frequency ranges. These results indicate that FR-4 is not only suitable in terms of electromagnetic performance, but also advantageous from a practical point of view due to its low cost, wide availability, and ease of fabrication. The obtained results further show that the proposed absorber exhibits a narrowband response, which may be attributed to the dominance of a single resonant mode supported by the selected unit-cell topology. This characteristic makes the design more suitable for applications requiring frequency-selective absorption rather than broadband suppression. In the present study, the performance of the proposed absorber was evaluated solely through full-wave electromagnetic simulations. Experimental validation through fabrication and measurement is considered a natural extension of this work and is planned for future investigation. Overall, the results confirm that the proposed FSS-based absorber successfully combines structural simplicity, low profile, and high absorption performance, making it a suitable candidate for X-band radar, satellite, and high-frequency communication systems.

## Conflict of Interest Statement

The authors declare that there is no conflict of interest

## Authorship Contribution Statement

**S.E.B.K:** Conceptualization, Methodology, Software, Formal analysis, Supervision, Investigation, Writing – Review & Editing; **C.G:** Visualization, Validation, Investigation, Software, Formal analysis, Writing – Original Draft; **E.T:** Visualization, Project administration, Supervision, Writing – Review & Editing

## References

[1] G. Chen, Z. Li, L. Zhang, Q. Chang, X. Chen, X. Fan, *et al*., "Mechanisms, design, and fabrication strategies for emerging electromagnetic wave-absorbing materials," *Cell Reports Physical Science*, vol. 5, no. 7, 2024. doi: 10.1016/j.xcrp.2024.102097

[2] A. S. Karim, "Simulation and experimental studies of broadband multi-resonators metamaterial absorber for satellite communications," *Bulletin of Materials Science*, vol. 47, no. 2, p. 114, 2024. doi: 10.1007/s12034-024-03182-8

[3] N. Liu, Z. Cui, S. Zhang, and L. Wang, "Ultra-wideband and multi-frequency switchable terahertz absorber based on vanadium dioxide," *Solid State Communications*, vol. 399, p. 115884, 2025. doi: 10.1016/j.ssc.2025.115884

[4] M. M. Tirkey and N. Gupta, "The quest for perfect electromagnetic absorber: A review," *International Journal of Microwave and Wireless Technologies*, vol. 11, no. 2, pp. 151–167, 2019. doi: 10.1017/S1759078718001472

[5] A. A. Abu Sanad, M. N. Mahmud, M. F. Ain, M. A. B. Ahmad, N. Z. B. Yahaya, and Z. Mohamad Ariff, "Theory, modeling, measurement, and testing of electromagnetic absorbers: A review," *physica status solidi (a)*, vol. 221, no. 4, 2024. doi: 10.1002/pssa.202300828

[6] A. Dhumal, M. S. Bisht, A. Bhardwaj, M. Saikia, S. Malik, and K. V. Srivastava, "Screen printed polarization independent microwave absorber for wideband RCS reduction," *IEEE Transactions on Electromagnetic Compatibility*, vol. 65, no. 1, pp. 96–103, 2022. doi: 10.1109/TEMC.2022.3213941

[7] Y. Xia, W. Gao, and C. Gao, "A review on graphene-based electromagnetic functional materials: Electromagnetic wave shielding and absorption," *Advanced Functional Materials*, vol. 32, no. 42, 2022. doi: 10.1002/adfm.202204591

[8] A. A. Abu Sanad, M. N. Mahmud, M. F. Ain, M. Hussien, M. A. Bin Ahmad, Z. M. Ariff, and N. Z. Yahaya, "The prospect of using hollow pyramidal microwave absorbers for 5G anechoic chamber applications: A review," *Journal of Applied Physics*, vol. 136, no. 23, 2024. doi: 10.1063/5.0244666

[9] M. Shehbaz, X. Li, C. Du, D. M. Xu, X. G. Yao, H. X. Lin, *et al*., "Materials engineering in microwave absorbers: Recent advances and prognosis," *Journal of Materials Chemistry C*, 2026. doi: 10.1039/D5TC02882E

[10] H. Huang, C. Hua, and Z. Shen, "Absorptive frequency-selective transmission structures based on hybrid FSS and absorber," *IEEE Transactions on Antennas and Propagation*, vol. 70, no. 7, pp. 5606–5613, 2022. doi: 10.1109/TAP.2022.3161472

[11] Priyanka, S. Mohanty, P. S. Alegaonkar, and H. B. Baskey, "Design and manufacturing of a hexapattern frequency selective surface absorber for aerospace stealth application," *ACS Applied Materials & Interfaces*, vol. 15, no. 30, pp. 37107–37115, 2023. doi: 10.1021/acsami.3c07669

[12] F. Che Seman, R. Cahill, V. F. Fusco, and G. Goussetis, "Design of a Salisbury screen absorber using frequency selective surfaces to improve bandwidth and angular stability performance," *IET Microwaves, Antennas & Propagation*, vol. 5, no. 2, pp. 149–156, 2011. doi: 10.1049/iet-map.2010.0072

[13] X. Liu, F. Xia, M. Wang, J. Liang, and M. Yun, "Working mechanism and progress of electromagnetic metamaterial perfect absorber," *Photonics*, vol. 10, no. 2, p. 205, Feb. 2023. doi: 10.3390/photonics10020205

[14] M. Qin, L. Zhang, and H. Wu, "Dielectric loss mechanism in electromagnetic wave absorbing materials," *Advanced Science*, vol. 9, no. 10, 2022. doi: 10.1002/advs.202105553

[15] Y. Akinay, U. Gunes, B. Çolak, and T. Cetin, "Recent progress of electromagnetic wave absorbers: A systematic review and bibliometric approach," *ChemPhysMater*, vol. 2, no. 3, pp. 197–206, 2023. doi: 10.1016/j.chphma.2022.10.002

[16] W. W. Salisbury, "Absorbent body for electromagnetic waves," U.S. Patent 2599944, 1952.

[17] B. J. E. L. Chambers, "Optimum design of a Salisbury screen radar absorber," *Electronics Letters*, vol. 30, no. 16, pp. 1353–1354, 1994. doi: 10.1049/el:1994089

[18] L. J. du Toit, "The design of Jauman absorbers," *IEEE Antennas and Propagation Magazine*, vol. 36, no. 6, pp. 17–25, Dec. 1994. doi: 10.1109/74.370526

[19] S. A. M. Ali, M. Abu, and S. N. Zabri, "A review: The development of metamaterial absorber," *International Journal of Integrated Engineering*, vol. 12, no. 1, pp. 72–80, 2020. doi: 10.30880/ijie.2020.12.01.007

[20] S. S. Bisht, A. Kumar, and D. K. Jhariya, "A review on electromagnetic metamaterial absorbers and its application," in *Compact and Flexible Microwave Devices*, 2025, pp. 151–195. doi: 10.1002/9781394275588.ch7

[21] S. Kalraiya, R. K. Chaudhary, M. A. Abdalla, and R. K. Gangwar, "Polarization and incident angle independent metasurface absorber for X-band application," *Materials Research Express*, vol. 6, no. 4, p. 045802, 2019. doi: 10.1088/2053-1591/aaf9ff

[22] B. Döken, "An easily optimizable frequency selective absorber design for X-band," *Afyon Kocatepe Üniversitesi Fen ve Mühendislik Bilimleri Dergisi*, vol. 22, no. 1, pp. 136–141, 2022. doi: 10.35414/akufemubid.823419

[23] Z. Yao, S. Xiao, Z. Jiang, L. Yan, and B. Z. Wang, "On the design of ultrawideband circuit analog absorber based on quasi-single-layer FSS," *IEEE Antennas and Wireless Propagation Letters*, vol. 19, no. 4, pp. 591–595, 2020. doi: 10.1109/LAWP.2020.2972919

[24] S. H. Behara, A. K. Gupta, K. Bammidi, S. D. Edubilli, A. Gatteem, and P. S. R. Chowdary, "Sierpinski gasket fractal-based microwave metamaterial absorber," in *2024 IEEE Wireless Antenna and Microwave Symposium (WAMS)*, 2024, pp. 1–4. doi: 10.1109/WAMS59642.2024.10528080

[25] A. Kumar, J. Padhi, G. S. Reddy, and S. Narayan, "Dual band polarization insensitive frequency selective surface absorber," in *2019 IEEE MTT-S International Microwave and RF Conference (IMARC)*, 2019, pp. 1–5. doi: 10.1109/IMaRC45935.2019.9118731

[26] L. Huang and H. Chen, "Multi-band and polarization insensitive metamaterial absorber," *Progress in Electromagnetics Research*, vol. 113, pp. 103–110, 2011. doi: 10.2528/PIER10122401

[27] Y. Li, P. F. Gu, Z. He, Z. Cao, J. Cao, K. W. Leung, and D. Ding, "An ultra-wideband multilayer absorber using an equivalent circuit-based approach," *IEEE Transactions on Antennas and Propagation*, vol. 70, no. 12, pp. 11911–11921, 2022. doi: 10.1109/TAP.2022.3213415

[28] B. Hu and T. Deng, "A broadband and wide-angle FSS absorber with vertical dipole array," in *2023 IEEE 11th Asia-Pacific Conference on Antennas and Propagation (APCAP)*, 2023. doi: 10.1109/APCAP59480.2023.10469904

[29] A. R. Bhamburkar and H. S. Sonalikar, "A wideband compact polarization-insensitive absorber using modified resistive Jerusalem cross FSS," in *2022 IEEE Microwaves, Antennas, and Propagation Conference (MAPCON)*, 2022. doi: 10.1109/MAPCON56011.2022.10046840

[30] S. Manokaran, S. J., R. Sivasamy, N. Surya V, and G. P., "An ultrathin FSS absorber for X-band applications," in *2024 Ninth International Conference on Science Technology Engineering and Mathematics (ICONSTEM)*, 2024. doi: 10.1109/ICONSTEM60960.2024.10568775

[31] J. Kumar, G. S. Padhi, R. Reddy, and S. Narayan, "FSS based wide band and polarization-insensitive EM wave absorber for RCS reduction application," in *2023 IEEE Wireless Antenna and Microwave Symposium (WAMS)*, 2023. doi: 10.1109/WAMS57261.2023.10242978

[32] N. Zabri, R. Cahill, and A. Schuchinsky, "Ultra-thin resistively loaded FSS absorber for polarisation independent operation at large incident angles," in *The 8th European Conference on Antennas and Propagation (EuCAP 2014)*, 2014, pp. 1363–1367. doi: 10.1109/EuCAP.2014.6902031

[33] L. Zheng, X. Yang, W. Gong, M. Qiao, and X. Li, "Ultralow thickness-bandwidth ratio magnetic absorber with printed FSS for S&C bands," *IEEE Antennas and Wireless Propagation Letters*, vol. 21, no. 3, pp. 576–580, Mar. 2021. doi: 10.1109/LAWP.2021.3138634

[34] M. Basravi, M. Maddahali, Z. H. Firouzeh, and A. Ramezani, "Design of a novel ultra broadband single-layer absorber using double fractal square loops," in *2016 24th Iranian Conference on Electrical Engineering (ICEE)*, 2016. doi: 10.1109/IranianCEE.2016.7585597

[35] J. da Silva Souza, A. J. R. Serres, and A. Gomes Neto, "A novel FSS absorber for 5 GHz WLAN applications," in *2022 IEEE International Symposium on Antennas and Propagation and USNC-URSI Radio Science Meeting (AP-S/USNC-URSI)*, 2022. doi: 10.1109/AP-S/USNC-URSI47032.2022.9886032

[36] M. Sainath, E. SreeLakshmi, and N. C. Pradhan, "Compact dual band FSS absorber with wider angular stability for C and X bands," in *2025 IEEE Microwaves, Antennas, and Propagation Conference (MAPCON)*, 2025. doi: 10.1109/MAPCON65020.2025.11426605

[37] S. Garg, R. K. Singh, R. Paliwal, and S. Yadav, "Dual-band FSS based microwave absorber for WiMAX & WLAN band applications," in *2021 IEEE Indian Conference on Antennas and Propagation (InCAP)*, 2021. doi: 10.1109/InCAP52216.2021.9726415

[38] P. Das and R. Panwar, "Analysis of a compact X-band metamaterial absorber," in *2021 IEEE International Conference on Electronics, Computing and Communication Technologies (CONECCT)*, 2021, pp. 1–5. doi: 10.1109/CONECCT52877.2021.9622542

[39] S. Luo, J. Zhao, D. Zuo, and X. Wang, "Perfect narrow band absorber for sensing applications," *Optics Express*, vol. 24, no. 9, pp. 9288–9294, 2016. doi: 10.1364/OE.24.009288

[40] S. Middha, I. Sharma, V. Arora, S. Singh, N. Tandon, H. S. Dosanjh, *et al.*, "rGO-tailored Ba–Sr hexaferrite composites for high-performance X-band microwave absorption and EMI shielding," *Journal of Materials Science*, pp. 1–24, 2026. doi: 10.1007/s10853-026-12278-x

[41] A. P. Sohrab and Z. Atlasbaf, "A circuit analog absorber with optimum thickness and response in X-band," *IEEE Antennas and Wireless Propagation Letters*, vol. 12, pp. 276–279, 2013. doi: 10.1109/LAWP.2013.2248073

[42] B. Syihabuddin, A. H. Gunawan, M. R. Effendi, and A. Munir, "Study on multilayer EM wave absorber composed of metasurface for X-band application," in *2019 IEEE International Conference on Communication, Networks and Satellite (Comnetsat)*, 2019, pp. 14–17. doi: 10.1109/COMNETSAT.2019.8844053

[43] A. H. Yuzer and E. Erdem, "Z shaped-based textile metamaterials absorber in X band," in *Proc. 3rd International Conference on Recent Academic Studies (ICRAS),* Konya, Türkiye, Dec. 03–04, 2024.

[44] R. Pelluri and B. Appasani, "Genetic algorithm optimized X-band absorber using metamaterials," *Progress in Electromagnetics Research Letters*, vol. 69, pp. 59–64, 2017. doi: 10.2528/PIERL17051902

[45] M. A. Abdalla and Z. Hu, "On the study of development of X band metamaterial radar absorber," *Advanced Electromagnetics*, vol. 1, no. 3, pp. 94–98, 2012. doi: 10.7716/aem.v1i3.25

[46] A. I. Dokumaci, F. Ö. Alkurt, L. Wang, and M. Karaaslan, "Metamaterial absorber-based rectifier circuit for efficient RF energy harvesting at 2.4 GHz for IoT applications," *Analog Integrated Circuits and Signal Processing*, vol. 124, no. 1, p. 8, 2025. doi: 10.1007/s10470-025-02412-1

[47] S. Ş. A. Madak, A. Teber, and R. Topkaya, "Polarization insensitive and thin metamaterial absorber performed in high-frequency 5G bands," *Journal of the Institute of Science and Technology*, vol. 14, no. 1, pp. 168–181, 2024. doi: 10.21597/jist.1300437

[48] Z. Ji, Y. Song, M. Gao, Q. Zhang, and Y. Liu, "Multimode miniature polarization-sensitive metamaterial absorber with ultra-wide bandwidth in the K band," *Micromachines*, vol. 15, no. 12, p. 1446, 2024. doi: 10.3390/mi15121446